CHINESE OPTICS LETTERS

Vol. 19, No. 12 | December 2021

Strong coupling with absorption and emission features of Ag@Au hollow nanoshells interacting with J-aggregated dye molecules

Tianchen Zhao (赵天琛)[1], Qiang Ma (马 强)[1], Yajie Bian (卞亚杰)[1], Yuyi Zhang (张钰伊)[1], Yiting Liu (刘易婷)[1], Xiaolei Zhang (张晓磊)[1,2*], Botao Wu (吴伯涛)[1**], E Wu (武 愕)[1,2], Shitao Lou (楼柿涛)[1], and Qingyuan Jin (金庆原)[1***]

[1] State Key Laboratory of Precision Spectroscopy, East China Normal University, Shanghai 200241, China

[2] Collaborative Innovation Center of Extreme Optics, Shanxi University, Taiyuan 030006, China

*Corresponding author: xlzhang@admin.ecnu.edu.cn

**Corresponding author: btwu@phy.ecnu.edu.cn

***Corresponding author: qyjin@phy.ecnu.edu.cn

Received March 25, 2021 | Accepted June 4, 2021 | Posted Online September 6, 2021

We investigate the strong coupling from 5,5′,6,6′-tetrachloro-1,1′-diethyl-3,3′-di(4-sulfobutyl)-benzimidazolocarbocyanine (TDBC) molecules near pure nano-triangular Ag prisms or Ag@Au hollow nanoshells. When TDBC molecules are deposited on pure Ag nanoprisms or Ag@Au hollow nanoshells with the plasmonic resonance peak, matching very closely with the absorption band of TDBC J-aggregates, obvious Rabi splitting can be observed due to the strong coupling regime. Meanwhile, the photoluminescence intensity decreased with the increasing of the temperature, verifying the decreasing plasmon–exciton coupling interaction in the higher temperature. Our experimental results are coincident with the simulation results calculated by finite-difference time-domain method.

Keywords: surface plasmon; nanoshells; plasmon–exciton coupling; Rabi splitting.

DOI: 10.3788/COL202119.123602

1. Introduction

Localized surface plasmon resonance (LSPR) is the collective resonance of the surface electrons of metal nanoparticles (NPs) when interacting with the electromagnetic field of incident light[1]. Based on the interaction between LSPR and nearby quantum emitters (atoms, molecules, quantum dots, etc.), a wealth of correlation effects and novel physical phenomena can be produced[2,3]. According to the strength, the coupling effects can be classified into weak and strong coupling regimes[4]. In strong coupling, electromagnetic modes generate a quick energy exchange with matter, which is faster than its mode damping, leading to modification of the spectroscopic response (two new normal modes), which is known as vacuum Rabi splitting[5]. In particular, strong coupling between LSPR in metal nanostructures and quantum emitters has become a hot spot in the field of quantum optics[6–10]. For strong coupling investigations, researchers have tried various types of nanostructures, such as Ag core-shell nanostructures[6], Ag nanoprisms[7], Ag nanorods[8], Au NPs[9], Ag nanoshells[10], and Ag@Au hollow nanoshells (HNSs)[4]. Among these metallic plasmonic configurations, the hybrid system of Ag@Au HNS and J-aggregated dyes is the ideal choice for the plasmon–excitons (plexcitons) coupling research, with the plasmon peak of the HNS tuned from 450 to 900 nm[11].

J-aggregates are the assemblies of molecules with a very intense, narrow absorption band (J band), which is red-shifted to a longer wavelength by comparison with the monomer absorption band[12]. Now, great scientific interest in J-aggregates has grown continuously. A large variety of cyanine dyes has been reported: 1,1'-diethyl-2,2'-cyanine (PIC), 5,5',6,6'-tetrachloro-1,1'-diethyl-3,3'-di(4-sulfobutyl)-benzimidazolocarbocyanine (TDBC), 1,1',3,3'-tetraethyl-5,5',6,6'-tetrachloro-benzimidazolocarbocyanine (TTBC), 3,3',9-triethyl-5,5'-dichlorothiacarbocyanine (TDC), 3,3'-bis(sulfopropyl)-5,5'-dichloro-9-ethylthiacarbocyanine (THIATS), and so on[13]. Among these dyes, TDBC has been the subject of a large number of investigations, including spectral properties and morphologies[14], photochemistry[15], and exciton dynamics[16]. This is due to the certain distinct advantage of TDBC, which does not require a high concentration to form J-aggregates in an aqueous solution at room temperature (RT). Moreover, the absorptivity in the peak of the J band is up to 600,000 $cm^2/mmol$ (per molecule in the

J-aggregate), which far exceeds the absorptivities of other known J-aggregating dyes[12].

In recent years, strong coupling systems based on metal nanostructures and J-aggregate systems have increasingly become a research hotspot in the field of nanoscience, including several research areas, such as the research on LSPR-based biosensors[6], light–matter interaction on the single-photon level[7], low-temperature strong coupling phenomena[17], and a length tunable optical microcavity[18]. Although strong coupling in the Ag@Au HNS/J-aggregate hybrid system has been reported[4], tunable plexcitons coupling of anisotropic noble metallic nano-triangular prisms and J-aggregated dyes with unique optical properties still needs further exploration.

In this paper, we choose the fairly stable J-aggregated TDBC molecules and the triangular Ag nanoprisms or Ag@Au HNS with excellent optical and structural properties to build the tunable plexcitons strong coupling system. In our experiments, Rabi splitting can be clearly observed in pure Ag NPs or Ag@Au HNS with J-aggregated dyes at RT, with the changing of the split peaks' intensities and positions due to the different LSPR modes of the two kinds of NPs. Moreover, the photoluminescence (PL) intensity tends to decrease with the increasing temperature, showing more prominent local field enhancement effects in the lower temperature. It indicates weaker coupling interaction between the metallic NPs and the dyes in the higher temperature, to a certain extent, identical with the results of temperature-dependent observations in the similar plexcitons coupling system reported previously[17].

2. Experimental Section

2.1. Sample preparation

2.1.1. Ag nanoprisms and Ag@Au HNS synthesis

The preparation of Ag nanoprisms is divided into seed preparation and particle synthesis. First, aqueous trisodium citrate (5 mL, 2.5 mmol/L), aqueous poly (sodium styrenesulphonate) (PSSS; 0.25 mL, 500 mg/L), and freshly prepared aqueous $NaBH_4$ (0.3 mL, 10 mmol/L) were mixed in the magnetic stirring process. Then, prepared aqueous $AgNO_3$ (5 mL, 0.5 mmol/L) was added at a speed of about 2 mL/min during stirring. After about 30 min, the solution changed to dark yellow, indicating that Ag NPs were formed. Secondly, the ascorbic acid (150 μL, 10 mmol/L) and seed solution of 500 μL prepared in the first step were added into 10 mL ultrapure water, and, then, the prepared aqueous $AgNO_3$ (6 mL, 0.5 mmol/L) was added at a speed of about 1 mL/min at the same time of stirring to synthesize Ag NPs with the LSPR at 567 nm. Finally, the Ag NPs were stabilized by the addition of aqueous trisodium citrate (1 mL, 25 mmol/L)[19].

The Ag@Au HNS synthesis was also completed in two steps. In the first step, 9 mL of Ag NPs solution were refluxed for 10 min. In the second step, the $HAuCl_4$ (130 μL, 3 mmol/L) aqueous solution was added dropwise. After that, we refluxed the mixture for 20 min until its color became stable. Vigorous magnetic stirring is necessary in these steps. The solution was then centrifuged with water twice (10,000 r/min, 7 min)[20].

2.1.2. Ag nanoprisms or Ag@Au HNS/J-aggregate hybrid fabrication

TDBC sodium salt was purchased from Shanghai Rechem science Co., Ltd. Ag@Au HNS/TDBC hybrid was produced by combining TDBC aqueous solution (2200 μL, 100 μmol/L) and 5 mL Ag@Au HNS solution under gentle magnetic stirring. In the same way, Ag NPs/TDBC hybrid was produced by combining TDBC aqueous solution (2500 μL, 100 μmol/L) and 6 mL Ag NPs solution under gentle magnetic stirring. After at least 24 h, both hybrid syntheses were centrifuged with water (10,000 r/min, 7 min) to remove excess TDBC dye molecules.

2.1.3. APTES functionalization

All of the samples were prepared in aqueous solution. Nevertheless, fluorescent spectra at low temperatures require them to be assembled on solid substrates. Now, we will explain how to assemble the hybrid nanostructures on a glass substrate[21]. The glass sheet was immersed in 3-aminopropyltriethoxysilane (APTES) for chemical functionalization of the self-assembled monolayers. This method is based on the covalent bonding of APTES molecules to hydroxyl terminated glass surfaces. As a result, positive charges are created at the glass surface. The functional glass substrate was immersed in the prepared metal particle solution and allowed to stand for 24 h, followed by nitrogen and ultrapure water cleaning.

2.2. Characterization

A PERSEE Tu-1901 instrument was used for the absorption spectral test. A liquid nitrogen cooled charge coupled device (CCD) with a spectrometer (Princeton Instruments) was used for the steady-state PL spectral detection. The PL was excited by a continuous light source (mercury lamp, setting the illumination wavelength at 532 nm). A microchannel plate photomultiplier tube (Hamamatsu) was used for photon counting. Transmission electron microscope (TEM) analysis was performed using a TECNAI G2F20 instrument, and scanning TEM (STEM) analysis was performed using a JEM2100F instrument; the samples were prepared by drop-casting 10 μL solution onto a Lacey Formvar/Carbon Film Coated Grids overnight and allowing the solvent (water) to evaporate naturally.

2.3. Simulations

The commercial software FDTD Solutions from Lumerical Solution, Inc., Canada, which is based on the finite-difference time-domain method, was used to simulate plexcitons coupling. A total field-scattered field source is injected onto Ag NPs or Ag@Au HNS without and with a TDBC shell, and the simulation wavelength ranges from 400 to 800 nm. The measured dielectric constants of Ag and Au are used in the simulation, which are included in Refs. [22,23], respectively. The optical properties of TDBC are described by a Lorentzian

function, $\varepsilon(\omega) = \varepsilon_0 - f\omega_0^2/(\omega_0^2 - \omega^2 - i\gamma_0\omega)$[24]. The thickness of the TDBC shell is taken as 3 nm with an oscillator strength of $f = 0.1$ and an exciton peak width of $\gamma_0 = 60.2$ meV, and its absorption line ω_0 is at 587 nm. The refractive index of the surrounding matrix is set to 1.33 for water ($\varepsilon_0 = 1.33$). The electric field distribution images around the NPs and HNS are extracted from the frequency domain field profile monitors. The region inside and around the NPs and HNS is meshed by a three-dimensional nonuniform grid with a size of 0.5 nm. To save the computational memory and time, perfectly matched layer absorption boundary conditions in the simulation region and symmetric boundary conditions for the NPs and HNS were used. Convergence testing was performed to assert the simulation results.

3. Results and Discussion

3.1. Experimental strong coupling of plasmons and excitons

The self-assembly processes of J-aggregated dyes in Ag nanoprisms and Ag@Au HNS are shown in Fig. 1(a). Figure 1(b) shows the chemical structure of a TDBC molecule. In the mixture of the NP colloidal solution and the TDBC solution, the citrate is adsorbed to the Au NPs surface through oxygen and can be easily replaced by TDBC molecules. So, the TDBC self-assembly is realized through ligand exchange reaction between the citrate and TDBC molecules[9].

The triangular edge structure of Ag nanoprisms and the Ag@Au HNS can be seen from the TEM images in Figs. 2(a) and 2(b) and the STEM images in Figs. 2(f) and 2(h). At first, Ag nano-triangular prisms were synthesized as the templates. When Au ions were added, the Ag atoms were replaced by electrochemical reduction (galvanic replacement reaction, GRR)[25]. Subsequently, the Au ions become Au atoms deposited on the surface of Ag NPs, as the Ag particles continue to participate by the GRR. The holes in the shell region serve as channels to help form the hollow Ag@Au nanostructures. The above point can be proved from the elemental maps shown in Figs. 2(e) and 2(g) and the EDX shown in Fig. 2(i) and Table 1. Fig. 2(c) shows the structure of TDBC-doped Ag nanoprisms,

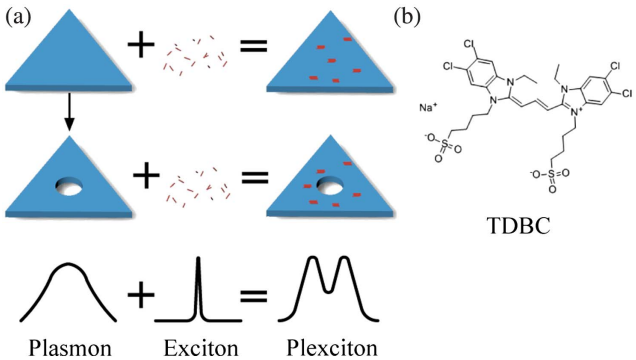

Fig. 1. (a) Schematic diagram of the hybrid of Ag nanoprisms and Ag@Au HNS embedded in an ensemble of J-aggregate (TDBC). (b) The structural formula of a TDBC molecule.

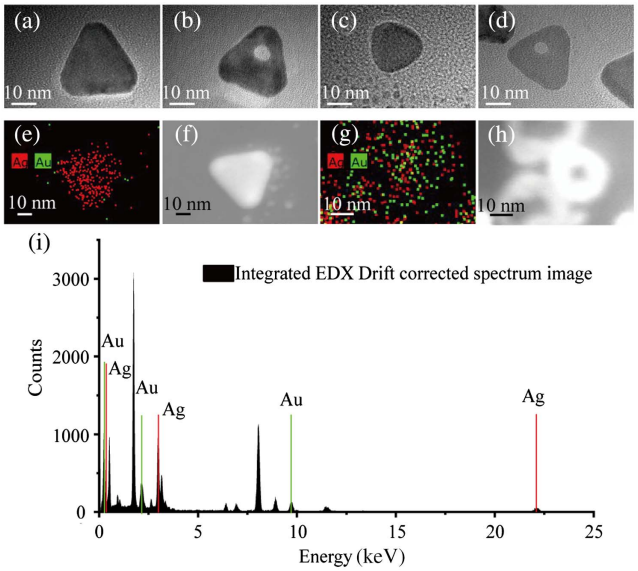

Fig. 2. TEM images of (a) Ag NPs, (b) Ag@Au HNS, (c) Ag NPs/TDBC, and (d) Ag@Au HNS/TDBC. (e) and (g) Mapping of elements (distribution of Ag/Au element) of Ag NPs and Ag@Au HNS. (f) and (h) STEM images of Ag NPs and Ag@Au HNS. (i) The energy dispersive X-ray spectroscopy (EDX) analysis of Ag@Au HNS.

and Fig. 2(d) shows the structure of TDBC-doped Ag@Au HNS. Since the J-aggregate absorption peak of TDBC dye molecules is around 587 nm [as shown in Fig. 3(a)], in order to help achieve strong Rabi splitting, the wavelength of LSPR of Ag@Au HNS is adjusted to 586 nm by accurately controlling the thickness of the Au shell, as shown in Fig. 3.

Figure 3(a) shows the absorption spectrum of TDBC dye molecules. The J-aggregate absorption peak is around 587 nm, which is consistent with the literatures[7,14]. From Fig. 3(b),

Table 1. EDX Spectrum Analysis of Ag@Au Hollow Nanostructure.

Element	Weight (%)	Atomic Fraction (%)
Ag	73.56	83.55
Au	26.44	16.45

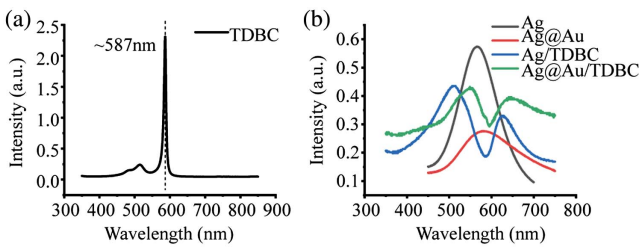

Fig. 3. (a) Ultraviolet-visible absorption spectrum of TDBC dye molecules. (b) Ultraviolet-visible absorption spectra of four nanostructures (black line indicates Ag NPs, red line indicates Ag@Au HNS, blue line indicates Ag NPs/TDBC, and green line indicates Ag@Au HNS/TDBC).

we can see that the LSPR of the Ag nanoprisms is located at 567 nm [the black line in Fig. 3(b)], not exactly matching the TDBC resonance band (587 nm). When the Ag nanoprisms interact with the excitons of TDBC, the absorption spectrum of the corresponding system (Ag NPs/TDBC) splits into a strong peak (512 nm, 2422 meV) and a weak peak (627 nm, 1978 meV), so the Rabi splitting is around 444 meV, as shown in the blue line in Fig. 3(b).

For the LSPR of Ag@Au HNS [586 nm, red line in Fig. 3(b)], whose mode matches the exciton peak of TDBC (587 nm), the strongly coupled hybrid exhibits obvious mode splitting. The absorption spectrum of the corresponding system (Ag@Au HNS/TDBC) splits into two new polariton peaks at 551 nm (2251 meV) and 647 nm (1917 meV), which exhibit comparable intensities. The Rabi splitting is around 334 meV, as shown in the green line in Fig. 3(b), which is smaller than that of Ag NPs/TDBC. Compared with solid core Ag nanoparticles, Ag@Au HNS has a unique voluminous void space, so it can improve radiation absorption efficiencies through "light trapping" effects. Simultaneously, the hollow materials can enhance light harvesting[26] and lead to different plasmon modes, which may cause a stronger coupling between Ag@Au HNS and TDBC than that between Ag NPs and TDBC.

Although the Rabi splitting of the absorption peak already indicates strong coupling between Ag NPs/Ag@Au HNS and TDBC, in order to better understand the physical mechanism involved, we adopt a more general strong coupling criterion[27,28]:

$$g^2 > \frac{\Gamma_{\mathrm{pl}}^2 + \gamma_0^2}{16}, \tag{1}$$

where g is the coupling strength, and Γ_{pl} and γ_0 are the full width at half-maximum (FWHM) line-widths of the plasmon and the exciton, respectively. When the inequality is satisfied, it can be thought that strong coupling has happened. The coupling strength g can be obtained by solving the following formula:

$$(\omega_+ - \omega_-)^2 = \sqrt{(\omega_{\mathrm{pl}} - \omega_0)^2(\Gamma_{\mathrm{pl}} - \gamma_0)^2 + \left[4g^2 + (\omega_{\mathrm{pl}} - \omega_0)^2 - \frac{(\Gamma_{\mathrm{pl}} - \gamma_0)^2}{4}\right]^2}, \tag{2}$$

where ω_{pl} is the energy level of LSPR, ω_0 is the energy level of the exciton, ω_+ is the energy level with high energy after coupling, called the upper branch, and ω_- is the energy level with low energy after coupling, called the lower branch. By using Eq. (2), the coupling strength g of the hybrid system of Ag NPs/TDBC is 241.7 meV, and the coupling strength g of the hybrid system of Ag@Au HNS/TDBC is 298.5 meV, both of which satisfy the inequality in Eq. (1), indicating that strong coupling has happened in both systems. The coupling strength of system 2 is greater than that of system 1, which shows that strong coupling between Ag NPs/Ag@Au HNS and TDBC is enhanced by the adjustment of the peak value.

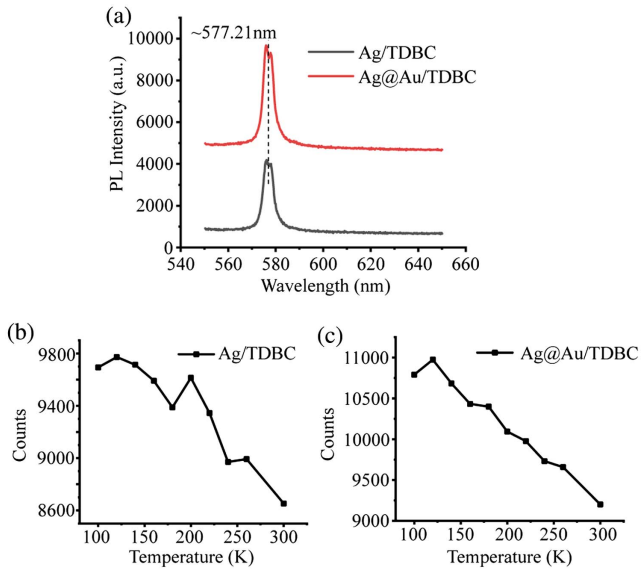

Fig. 4. (a) Fluorescent spectra of Ag NPs/TDBC and Ag@Au HNS/TDBC. (b), (c) Temperature-dependent fluorescence intensity curves of Ag NPs/TDBC and Ag@Au HNS/TDBC measured at T = 100–300 K.

The fluorescent spectra of the hybrid system of Ag NPs/TDBC and Ag@Au HNS/TDBC at RT are shown in Fig. 4(a). The fluorescence peaks of the two systems are both around 577 nm. Figures 4(b) and 4(c) show the variation curves of the intensity of the hybrid system of Ag NPs/TDBC and Ag@Au HNS/TDBC when the temperature gradually decreases from RT (300 K) to 100 K. In Fig. 4(b), the fluorescence intensity of the hybrid system of Ag NPs/TDBC shows an upward trend as the temperature decreases. At certain temperatures (240 K, 180 K, and 100 K), there will be a downward trend, but the overall trend remains rising. In Fig. 4(c), the fluorescence intensity of the hybrid system of Ag@Au HNS/TDBC also shows an upward trend with the decrease of temperature. At a certain temperature (only 100 K), there will be a downward trend. But, the overall trend keeps rising. It can be seen that when the temperature gradually decreases, there appears to be more local field enhancement. Up to a certain extent, the results illustrate that the coupling between Ag NPs/Ag@Au HNS and TDBC is strongly affected by temperature changes, similar to literature information[17].

3.2. Simulated strong coupling of plasmons and excitons

To explain the observed positions and intensities of the absorption peaks varying with the LSPR modes and the structures of the Ag NPs or Ag@Au HNS with J-aggregated dyes, the near field distributions for the two systems were simulated using the FDTD method. As shown in Figs. 5(a)–5(h), strong electric fields ($|E/E_0|$) are observed around the surfaces of Ag NPs and Ag@Au HNS, and Rabi splitting can also be clearly observed in the hybrid nanostructures. It should be noted that the simulation spectra of four nanostructures are a little different from those obtained in the experiment. This can be mainly ascribed to

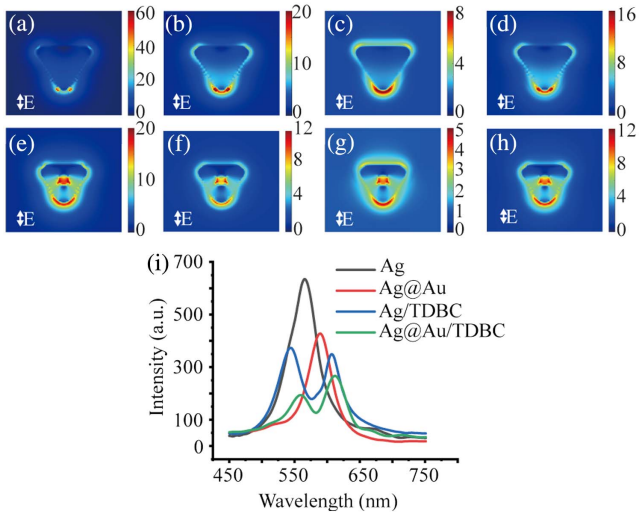

Fig. 5. Electric field ($|E/E_0|$) distribution images for the (a) pure Ag individual NP with LSPR peak at 565 nm, (b) TDBC-doped Ag NPs ensemble with LSPR peak at the upper branch (ω_+) maximum (544 nm), (c) TDBC-doped Ag NPs ensemble with LSPR peak at the minimum (577 nm), (d) J-aggregate-doped Ag NPs ensemble with LSPR peak at the lower branch (ω_-) maximum (607 nm), (e) Ag@Au HNS individual nanoparticle with LSPR peak at 589 nm, (f) TDBC-doped Ag@Au HNS ensemble with LSPR peak at the upper branch (ω_+) maximum (559 nm), (g) TDBC-doped Ag@Au HNS ensemble with LSPR peak at the minimum (583 nm), and (h) J-aggregate-doped Ag@Au HNS ensemble with LSPR peak at the lower branch (ω_-) maximum (612 nm). (i) Simulation extinction spectra of four nanostructures (black line indicates Ag NPs, red line indicates Ag@Au HNS, blue line indicates Ag NPs/TDBC, and green line indicates Ag@Au HNS/TDBC).

the ideal models of theoretical simulations and the irregular shape of Ag NPs and Ag@Au HNS in the experiment.

4. Conclusion

In summary, bimetallic HNSs with controlled LSPR were synthesized. After TDBC molecules were deposited on the bimetallic HNS, the absorption spectra and PL spectra were studied. Strong coupling was observed by precisely adjusting the LSPR of NPs to match the molecular absorption band; meanwhile, the coupling phenomenon is stronger than that of Ag nanoprisms. In the variable temperature experiment, the coupling strength can be inferred by observing the change of PL intensity, which tends to decrease with the temperature increasing. Finally, the strong coupling experimental results have been successfully verified by the FDTD simulation.

Acknowledgement

This work was supported by the National Key R&D Program of China (No. 2017YFA0303403), the National Natural Science Foundation of China (Nos. 11874015, 12074012, 11674099, and 11722431), the Shanghai International Cooperation Project (No. 16520710600), and the Program of Introducing Talents of Discipline to Universities (No. B12024).

References

1. L. J. Sherry, R. C. Jin, C. A. Mirkin, G. C. Schatz, and R. P. Van Duyne, "Localized surface plasmon resonance spectroscopy of single silver triangular nanoprisms," Nano Lett. **6**, 2060 (2006).
2. Q. Zhang, J. J. Ren, X. K. Duan, H. Hao, Q. H. Gong, and Y. Gu, "Enhancing coupling coefficient in a hybrid nanotoroid-nanowire system," Chin. Opt. Lett. **17**, 032702 (2019).
3. X. R. Ma, H. Cheng, J. W. Hou, G. H. Wu, X. Y. Lü, X. X. Zheng, and C. Chen, "Detection of breast cancer based on novel porous silicon Bragg reflector surface-enhanced Raman spectroscopy-active structure," Chin. Opt. Lett. **18**, 051701 (2020).
4. L. C. Sun, Z. Li, J. S. He, and P. J. Wang, "Strong coupling with directional absorption features of Ag@Au hollow nanoshell/J-aggregate heterostructures," Nanophotonics **8**, 1835 (2019).
5. D. G. Baranov, M. Wersall, J. Cuadra, T. J. Antosiewicz, and T. Shegai, "Novel nanostructures and materials for strong light–matter interactions," ACS Photonics **5**, 24 (2018).
6. Y. K. Tang, X. T. Yu, H. F. Pan, J. Q. Chen, B. Audit, F. Argoul, S. J. Zhang, and J. H. Xu, "Numerical study of novel ratiometric sensors based on plasmon–exciton coupling," Appl. Spectrosc. **71**, 2377 (2017).
7. G. Zengin, M. Wersäll, S. Nilsson, T. J. Antosiewicz, M. Käll, and T. Shegai, "Realizing strong light–matter interactions between single-nanoparticle plasmons and molecular excitons at ambient conditions," Phys. Rev. Lett. **114**, 157401 (2015).
8. G. Zengin, G. Johansson, P. Johansson, T. J. Antosiewicz, M. Käll, and T. Shegai, "Approaching the strong coupling limit in single plasmonic nanorods interacting with J-aggregates," Sci. Rep. **3**, 3074 (2013).
9. D. D. Lekeufack, A. Brioude, A. W. Coleman, P. Miele, J. Bellessa, L. D. Zeng, and P. Stadelmann, "Core-shell gold J-aggregate nanoparticles for highly efficient strong coupling applications," Appl. Phys. Lett. **96**, 253107 (2010).
10. N. Zhou, M. Yuan, Y. H. Gao, D. S. Li, and D. R. Yang, "Silver nanoshell plasmonically controlled emission of semiconductor quantum dots in the strong coupling regime," ACS Nano **10**, 4154 (2016).
11. W. D. Ma, H. F. Yang, Z. P. Li, S. Kulkarni, D. Zhang, L. S. Zhang, Y. Fang, and P. J. Wang, "The tunable and well-controlled surface plasmon resonances of Au hollow nanostructures by a chemical route," Plasmonics **13**, 47 (2018).
12. J. Moll, S. Daehne, J. R. Durrant, and D. A. Wiersma, "Optical dynamics of excitons in J aggregates of a carbocyanine dye," J. Chem. Phys. **102**, 6362 (1995).
13. F. Würthner, T. E. Kaiser, and C. R. Saha-Möller, "J-aggregates: from serendipitous discovery to supramolecular engineering of functional dye materials," Angew. Chem. Int. Ed. **50**, 3376 (2011).
14. A. V. Sorokin, I. Y. Ropakova, R. S. Grynyov, M. M. Vilkisky, V. M. Liakh, I. A. Borovoy, S. L. Yefimova, and Y. V. Malyukin, "Strong difference between optical properties and morphologies for J-Aggregates of similar cyanine dyes," Dyes Pigm. **152**, 49 (2018).
15. B. Munkhbat, M. Wersäll, D. G. Baranov, T. J. Antosiewicz, and T. Shegai, "Suppression of photo-oxidation of organic chromophores by strong coupling to plasmonic nanoantennas," Sci. Adv. **4**, eaas9552 (2018).
16. A. V. Sorokin, I. Y. Ropakova, S. Wolter, R. Lange, I. Barke, S. Speller, S. L. Yefimova, Y. V. Malyukin, and S. Lochbrunner, "Exciton dynamics and self-trapping of carbocyanine J-aggregates in polymer films," J. Phys. Chem. C. **123**, 9428 (2019).
17. M. Wersall, B. Munkhbat, D. G. Baranov, F. Herrera, J. S. Cao, T. J. Antosiewicz, and T. Shegai, "Correlative dark-field and photoluminescence spectroscopy of individual plasmon–molecule hybrid nanostructures in a strong coupling regime," ACS Photonics **6**, 2570 (2019).
18. C. E. Finlayson, G. Vijaya Prakash, and J. J. Baumberg, "Strong exciton-photon coupling in a length tunable optical microcavity with J-aggregate dye heterostructures," Appl. Phys. Lett. **86**, 041110 (2005).
19. D. Aherne, D. M. Ledwith, M. Gara, and J. M. Kelly, "Optical properties and growth aspects of silver nanoprisms produced by a highly reproducible

and rapid synthesis at room temperature," Adv. Funct. Mater. **18**, 2005 (2008).
20. Y. G. Sun and Y. N. Xia, "Mechanistic study on the replacement reaction between silver nanostructures and chloroauric acid in aqueous medium," J. Am. Chem. Soc. **126**, 3892 (2004).
21. S. Balci, "Ultrastrong plasmon–exciton coupling in metal nanoprisms with J-aggregates," Opt. Lett. **38**, 4498 (2013).
22. D. W. Lynch and W. R. Hunter, *Handbook of Optical Constants of Solids* (Academic, 1985), p. 350.
23. J. Carper, "The CRC handbook of chemistry and physics," Libr. J. **124**, 192 (1999).
24. M. Wersall, J. Cuadra, T. J. Antosiewicz, S. Balci, and T. Shegai, "Observation of mode splitting in photoluminescence of individual plasmonic nanoparticles strongly coupled to molecular excitons," Nano Lett. **17**, 551 (2017).
25. C. M. Cobley and Y. N. Xia, "Engineering the properties of metal nanostructures via galvanic replacement reactions," Mater. Sci. Eng. **70**, 44 (2010).
26. G. Prieto, H. Tüysüz, N. Duyckaerts, J. Knossalla, G. H. Wang, and F. Schüth, "Hollow nano- and microstructures as catalysts," Chem. Rev. **116**, 14056 (2016).
27. E.-M. Roller, C. Argyropoulos, A. Högele, T. Liedl, and M. Pilo-Pais, "Plasmon–exciton coupling using DNA templates," Nano Lett. **16**, 5962 (2016).
28. B. W. Shore and P. L. Knight, "The Jaynes–Cummings model," J. Mod. Opt. **40**, 1195 (1993).